Proceedings of 5th Jagiellonian Symposium on Advances in Particle Physics and Medicine, Kraków, Poland, 2024

The ηd Interaction Studied in $\gamma d \to \pi^0 \eta d$

T. Ishikawa*

Research Center for Nuclear Physics (RCNP), Osaka University, Ibaraki 567-0047, Japan

Doi: 10.12693/APhysPolA.146.687 *e-mail: ishikawa@rcnp.osaka-u.ac.jp

We have studied the interaction between the eta meson and deuteron (ηd interaction) from measurement of cross-sections for coherent neutral-pion and eta-meson photoproduction on the deuteron ($\gamma d \to \pi^0 \eta d$) using the photon beam at the Research Center for Electron Photon Science (ELPH), Tohoku University, Japan. We have found a narrow resonance-like peak in the ηd subsystem in the vicinity of the threshold, suggesting strong ηd attraction. The sharp backward-peaking angular dependence of deuteron emission, predicted by the existing theoretical calculations, does not appear. We discuss a possible production mechanism of the $\gamma d \to \pi^0 \eta d$ reaction and the possibility of using coherent π^0 and η photoproduction on a nucleus to study the η-nuclear interaction.

topics: ηd interaction, dibaryonic resonance, coherent meson photoproduction

1. Introduction

How is the matter existing around us composed, how was it born, and how does it evolve? To approach this fundamental mystery of the universe, we have been pursuing the smallest building blocks, "elementary particles," by breaking down matter. Now we know that elementary particles, quarks and gluons, form the first matter "hadrons," such as protons and neutrons (collectively called nucleons) that make up atomic nuclei. Quarks and gluons moving freely in the early universe formed hadrons, being confined within them as the temperature decreases and interaction becomes stronger, acting on quarks and gluons. The mass of a hadron is much larger than the sum of masses of quarks comprising it. The hadron formation led to the generation of a large amount of matter mass and made the first step in the evolution of matter. Since quarks and gluons cannot be observed alone owing to their confinement, their dynamics can only be studied through hadronic phenomena.

Hadron–hadron interaction provides crucial insight into quantum chromodynamics (QCD), a fundamental theory of strong interaction, in the non-perturbative regime. A hadron is considered an excitation of the QCD vacuum described by various non-vanishing condensates. Chiral symmetry breaking is considered to be responsible for making $\langle \bar{q}q \rangle$ condensate, which plays a role as resistance for moving quarks and thus dynamical mass generation of hadrons. The condensate depends on the environment, temperature, and density. We can expect a finite decrease in the condensate inside a nucleus, leading to a decrease in hadron masses.

This scenario also predicts the existence of the chiral partner of a hadron with the same mass and the same quantum numbers except for the parity at the chiral limit, where chiral symmetry is not breaking and $\langle \bar{q}q \rangle$ condensate is absent. Currently, the $N(1535)1/2^-$ nucleon resonance is speculated to be the chiral partner of the nucleon. Therefore, the nucleon (N) and $N^* \equiv N(1535)1/2^-$ are expected to degenerate, leading to a decrease in the mass difference between N and N^* as the chiral condensate decreases [1, 2]. Since N^* strongly couples to the η meson and nucleon in free space, the η meson is a mixed state between the pure η state and N^*-particle and N-hole (N^*-N) state. The pure η state is lower by 48 MeV than the N^*-N state, leading to an attractive η-nuclear force. In a nucleus, the pure η state could be higher than the N^*-N state owing to the degeneration of N^* and N, leading to a repulsive η-nuclear force. This level crossing gives rise to both the η-nuclear bound states and resonant states when η mesons are produced in a nucleus [3, 4]. We can observe neither of them if the decrease in chiral condensate is not large enough and the level crossing does not take place in a nucleus. Currently, no clear evidence is obtained for an η-nuclear state for light nuclei [5, 6]. It is necessary to study η-nuclear interactions in more detail [7].

A traditional tool for studying the η-nuclear interaction is single η production from a nucleus. A significant increase in the η yield at low relative η-nuclear momenta observed in the reactions $pd \to \eta^3\mathrm{He}$ [8], $dp \to \eta^3\mathrm{He}$ [9, 10], $\gamma^3\mathrm{He} \to \eta^3\mathrm{He}$ [11–13], $\gamma^7\mathrm{Li} \to \eta^7\mathrm{Li}$ [14, 15] is interpreted as a signature of attractive forces between the η and nucleus.

A significant amount of information on the low-energy η-nuclear dynamics has been obtained from the final-state interactions in the $pn \to \eta d$ [16, 17] and $pd \to \eta pd$ [18, 19] reactions. Despite large cross-sections of these hadronic processes, their analysis can be complicated by various ambiguities associated with the initial-state interaction and dominance of various two-step mechanisms, leading to undesirable model dependence.

These disadvantages are overcome by turning to electromagnetic processes where it is not necessary to consider the initial state interaction. The coherent photoproduction of $\pi^0\eta$ pairs on a nucleus, $\gamma A \to \pi^0\eta A$, is especially suitable for studying the η-nuclear interaction. Although there are three hadrons in the final state, a condition of low eta deuteron relative momentum can be provided. The π^0-nuclear interaction is expected to result in a trivial small decrease in the π^0 yield due to absorption by the residual nucleus. The $\pi^0\eta$ interaction is small, at least at low energies below $a_0(980)$. Furthermore, the underlying elementary process $\gamma N \to \pi^0\eta N$ is rather well understood, where the excitation of the $\Delta(1700)3/2^-$ and $\Delta(1940)3/2^-$ resonances is followed by their decay into $\eta\Delta$ and successively into the final $\pi^0\eta N$ state. We have studied the ηd interaction from the $\gamma d \to \pi^0\eta d$ reaction at first, although level crossing is not expected owing to the low density of a small nuclear system, the deuteron. The results shown in this manuscript are based on the published papers [20, 21].

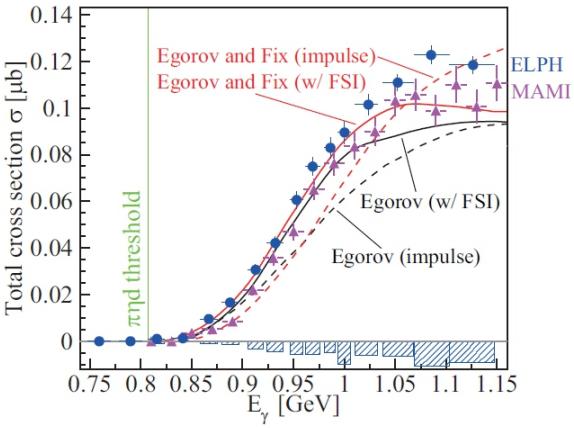

Fig. 1. Total cross-section σ as a function of the incident photon energy E_γ. The blue circles show σ obtained in the ELPH facility [20, 21], and the magenta triangles obtained in another facility in Mainz [34]. The lower hatched histogram shows the systematic uncertainty considered in [20, 21]. The data are compared with the existing calculations [35, 36]. The red curves show the calculations by Egorov and Fix [35], and the black show those by Egorov [36]. The dotted curves represent the calculations based on the impulse approximation, namely mesons are produced from the participant nucleon. The calculation by Egorov also includes the pion scattering $\pi^\pm N \to \eta N'$ and pion absorption $\pi^\pm N \to N'$ on the spectator nucleon. The solid curves incorporate the meson nucleon final-state interaction effects.

2. Experiment

A series of meson photoproduction experiments [22] were carried out using a bremsstrahlung photon beam [23–26] at the Research Center for Electron Photon Science (ELPH), Tohoku University, Japan [27], which was reorganized into the Research Center for Accelerator and Radio Isotope Science (RARiS) [28] on April 1, 2024. Bremsstrahlung photons were produced from 1.20 GeV circulating electrons in a synchrotron, called the STretcher Booster (STB) ring [29], by inserting a carbon wire. The photon energy, ranging from 0.75 to 1.15 GeV, was determined by detecting the post-bremsstrahlung electron with a photon-tagging counter, called the STB-Tagger II [23].

The target used was liquid deuterium with a thickness of 45.9 mm. All the final-state particles in the $\gamma d \to \pi^0\eta d \to \gamma\gamma\gamma\gamma d$ reaction were measured with the Four-pi Omni-directional Response Extended Spectrometer Trio (FOREST) detector [30] consisting of three different electromagnetic calorimeters (EMCs): pure cesium iodide crystals in the forward region, lead and scintillating fiber modules in the central, and lead glass counters in the back. A plastic-scintillator hodoscope (PSH) was placed in front of each EMC to identify charged particles. The forward PSH could determine their impact positions precisely without using information from the corresponding EMC. The trigger condition of the data acquisition required the detection of multiple particles in coincidence with a photon-tagging signal.

3. Analysis

At first, we select the events containing four neutral particles as candidates for four photons and a charged particle as a candidate for the deuteron. To reject neutrons, we require the same time response between any two neutral clusters out of four. The deuteron is detected with the forward PSH, and the time delay is required to be longer than 1 ns with respect to the timing response of the four neutral particles. The energy deposit is also required to be greater than twice that of the minimum ionizing particles. We utilize a sideband background subtraction method to remove accidental coincidence between photon detection with the FOREST detector and electron detection with the STB-Tagger II counters.

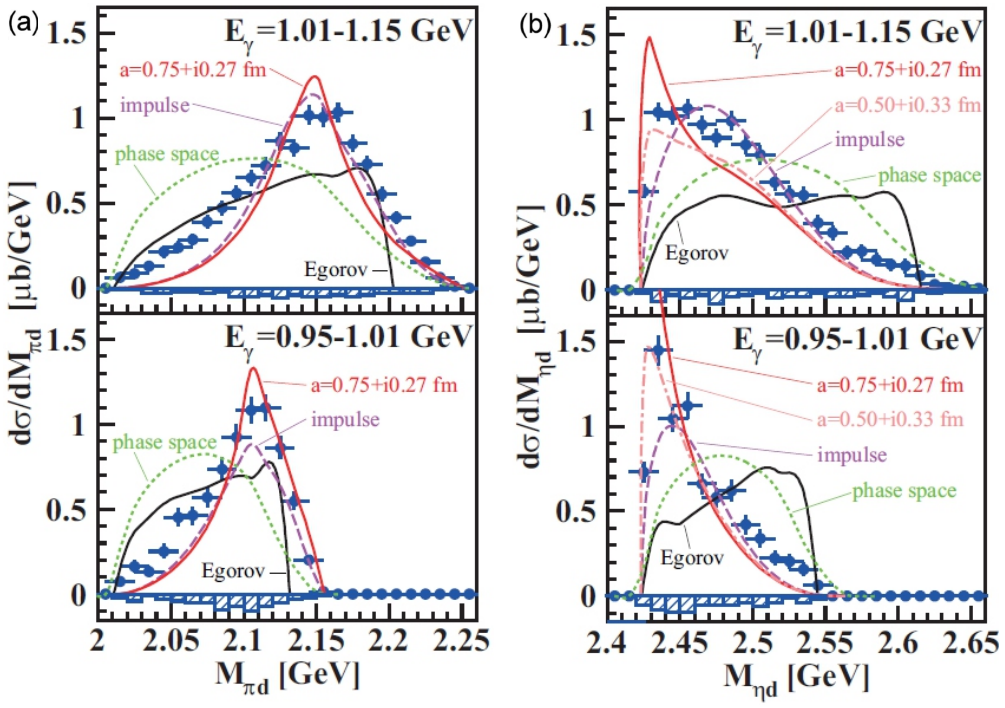

Fig. 2. Differential cross-sections $\mathrm{d}\sigma/\mathrm{d}M_{\pi d}$ (a) and $\mathrm{d}\sigma/\mathrm{d}M_{\eta d}$ (b). The top panels show the data at E_γ = 1.01–1.15 GeV, and the bottom panels show those at E_γ = 0.95–1.01 GeV. The lower hatched histograms are the corresponding systematic errors. The green dotted curves represent the pure phase space, which is normalized so that the corresponding total cross-section meets the measured one. The magenta dashed, red solid, and orange dot-dashed curves show, respectively, the impulse-approximation calculations, the full calculations with the set of the ηN parameters corresponding to $a_{\eta N} = 0.75 + \mathrm{i}0.27$ fm, and those with $a_{\eta N} = 0.50 + \mathrm{i}0.33$ fm ($\mathrm{d}\sigma/\mathrm{d}M_{\eta d}$ only) by Egorov and Fix [35]. The black solid curves show the full calculations by Egorov [36].

For the further event selection, we apply a kinematical fit with six constraints for the $\gamma d \to \pi^0 \eta d$ reaction: energy and momentum conservation between the initial and final states provides four constraints, with each two-photon invariant mass being the rest mass of the neutral pion or eta meson providing one, namely two in total. The events are selected with a χ^2 probability higher than 0.2 to remove the background processes. Additionally, quasi-free $\gamma p \to \pi^0 \eta p$ events are removed by using a kinematic fit with the corresponding hypothesis.

4. Results

The cross-sections were obtained by estimating the number of effective incident photons, the number of target deuterons, and the acceptance of $\gamma\gamma\gamma\gamma d$ detection in a Monte Carlo simulation based on Geant4 [31–33]. Here, event generation was modified from pure phase space to reproduce the following three measured distributions: the $\pi^0 d$ invariant mass $M_{\pi d}$, the ηd invariant mass $M_{\eta d}$, and the deuteron emission angle $\cos(\theta_d)$ in the γd center-of-mass (CM) frame.

4.1. Total cross-section

Figure 1 shows the total cross-section σ as a function of the incident photon energy E_γ (excitation function) together with the results from Mainz [34]. The data are compared with the existing theoretical calculations [35, 36]. The calculations are based on the impulse approximation, namely mesons are produced from the participant nucleon. The calculation by Egorov also includes the pion scattering $\pi^\pm N \to \eta N'$ and pion absorption $\pi^\pm N \to N'$ on the spectator nucleon. Both the calculations also incorporate the meson nucleon final-state interaction effects. Here, the ηd interaction plays a dominant role, as shown in threshold enhancements of $\mathrm{d}\sigma/\mathrm{d}M_{\eta d}$.

4.2. Differential cross-sections

Figure 2a shows the differential cross-sections $\mathrm{d}\sigma/\mathrm{d}M_{\pi d}$ ($M_{\pi d}$ — invariant mass distribution), exhibiting a peak at around the sum of the N and Δ masses. This suggests that quasi-free Δ production takes place or a ΔN correlated state is produced.

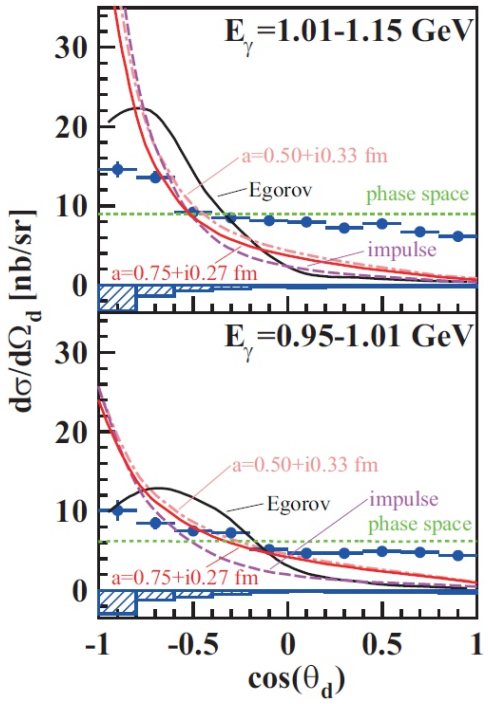

Fig. 3. Angular differential cross-sections $\mathrm{d}\sigma/\mathrm{d}\Omega_d$. The top panel shows the data at $E_\gamma = 1.01$–1.15 GeV, and the bottom panel shows those at $E_\gamma = 0.95$–1.01 GeV. The lower hatched histograms are the corresponding systematic errors. The green dotted curves represent the pure phase space, which is normalized so that the corresponding total cross-section meets the measured one. The magenta dashed, red solid, and orange dot-dashed curves show the impulse-approximation calculations and the full calculations with the set of the ηN parameters corresponding to $a_{\eta N} = 0.75 + \mathrm{i}0.27$ fm by Egorov and Fix [35]. The black solid curves show the full calculations by Egorov [36].

The calculations by Egorov and Fix reproduce this behavior well, although some discrepancies can be observed at low masses. On the other hand, the calculations by Egorov do not reproduce it completely.

Figure 2b shows the differential cross-section $\mathrm{d}\sigma/\mathrm{d}M_{\eta d}$ ($M_{\eta d}$ — invariant mass distribution), showing a prominent peak near the ηd threshold. The S-wave attraction between the η and deuteron is responsible for this peak, where the low relative momenta condition satisfies the ηd system. The calculations by Egorov and Fix well reproduce this behavior when the ηd final-state interactions are incorporated in terms of the $a_{\eta N}$ scattering length. The best $a_{\eta N}$ to reproduce the $M_{\eta d}$ invariant mass distribution is $a_{\eta N} = 0.50 + \mathrm{i}0.33$ fm. The calculations by Egorov do not reproduce the $M_{\eta d}$ distribution, especially the rapid rise of $\mathrm{d}\sigma/\mathrm{d}M_{\eta d}$ at low ηd relative momenta.

Figure 3 shows the angular distribution of deuteron emission $\mathrm{d}\sigma/\mathrm{d}\Omega$ in the center-of-mass frame, which is rather uniform, similar to those obtained in the $\gamma d \to \pi^0\pi^0 d$ reaction. Both the calculations by Egorov and Fix and those by Egorov do not reproduce this behavior. The former show strongly backward-peaking distributions. The latter do not show such behavior. The common feature of the theoretical calculations is very small $\mathrm{d}\sigma/\mathrm{d}\Omega_d$ at forward angles. This would suggest that the $\gamma d \to \pi^0\eta d$ reaction can not be described in a coherent sum of elementary amplitudes and that some two-baryon correlated state shows up in each step of meson emission. The FOREST detector does not include the magnetic spectrometer, thus the particle identification power of the forward-going deuteron is questionable. Yet, recent results from the BGOOD (BGO-Open Dipole) experiment, which possesses the dipole magnetic spectrometer at forward angles, also give completely consistent differential cross-sections $\mathrm{d}\sigma/\mathrm{d}\Omega$ at forward angles ($\cos(\theta) > 0.8$) of deuteron emission in the center-of-mass frame [37]. Completely different angular distributions are obtained in experiments. This does not suggest that a simple coherent sum of elementary amplitudes reproduces the data. Afterward, new calculations for $\gamma d \to \pi^0\eta d$, which incorporate various diagrams including pion scattering on the spectator nucleon and triangle singularity, try to interpret the $\gamma d \to \pi^0\eta d$ reactions [38]. Although the invariant mass distributions are well reproduced, the uniform angular distribution of deuteron emission cannot be reproduced.

Currently, no convincing evidence for an η-mesic nucleus has yet been obtained. Coherent photoproduction of π^0 and η pairs from nuclei would be a suitable reaction to access possible η-mesic nuclei. The effects of strong η-nuclear attraction can be observed in the vicinity of the threshold in the η-nuclear invariant mass distributions.

4.3. Phenomenological analysis of $a_{\eta d}$

We have decomposed the obtained πd and ηd invariant-mass distributions to these two sequential processes

$$\gamma d \to \mathcal{R}_{\pi\pi d} \to \pi^0 \mathcal{R}_{\eta d} \to \pi^0 \eta d, \tag{1}$$

and

$$\gamma d \to \mathcal{R}_{\pi\pi d} \to \eta \mathcal{R}_{\pi d} \to \pi^0 \eta d, \tag{2}$$

where $R_{\pi\pi d}$ denotes the first intermediate state, $R_{\eta d}$ and $R_{\pi d}$ denote the S-wave ηd system with a spin-parity of 1^-, and ΔN is a correlated state. Here, $R_{\eta d}$ may be an S-wave nucleon and $N(1535)1/2^-$ molecule-like state, while $R_{\pi d}$ is known as a resonance with spin-parity 2^+, mass ≈ 2.14 GeV, and width ≈ 0.09 GeV. We use a Breit–Wigner shape with a constant M and constant Γ for $R_{\pi d}$, and the complex scattering parameters (scattering length $a_{\eta d}$, effective range $r_{\eta d}$) in an effective range expansion for the reproduction of the $R_{\eta d}$ contribution. We perform a simultaneous fit of

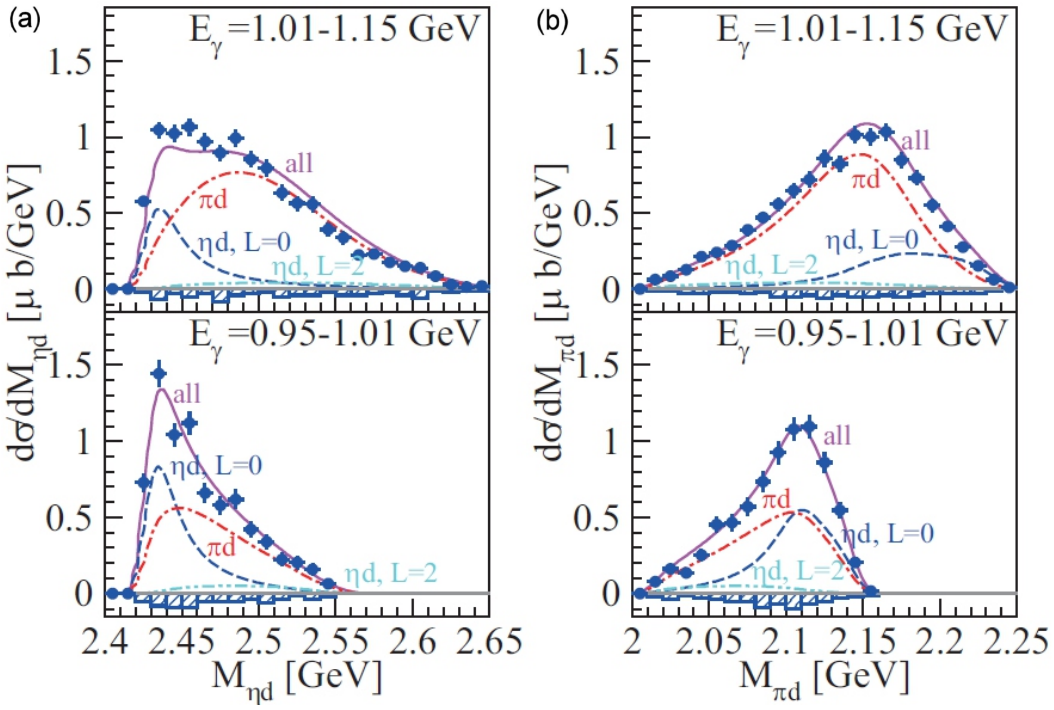

Fig. 4. Differential cross-sections $d\sigma/dM_{\eta d}$ (a) and $d\sigma/dM_{\pi d}$ (a) together with the fitted functions (magenta solid curves). The top panels show the data at E_γ = 1.01–1.15 GeV, and the bottom panels show those at E_γ = 0.95–1.01 GeV. The blue dashed and cyan double-dotted curves show, respectively, the S- and D-wave decay contributions of $R_{\eta d}$. The red dot-dashed curves represent the contribution from $R_{\pi d}$.

the πd and ηd invariant-mass distributions at two incident photon energies to determine these six parameters. Here, the D-wave decay of the $R_{\eta d}$ system is also considered by modifying the yields depending on the invariant mass ηd, namely the phase volume. Figure 4 shows $d\sigma/dM_{\eta d}$ and $d\sigma/dM_{\pi d}$ together with the fitted functions and their components. The obtained parameters are

$$a_{\eta d} = \pm\left(0.7^{+0.8}_{-0.6}\right) + \mathrm{i}\left(0.0^{+1.5}_{-0.0}\right), \quad (3)$$

and

$$r_{\eta d} = \mp\left(4.3^{+8.6}_{-2.9}\right) + \mathrm{i}\left(6.7^{+6.0}_{-8.4}\right) \quad (4)$$

with $\chi^2 = 131.3$ for 76 data points, where the double signs correspond to each other. The possible parameter region is very wide, but the obtained scattering parameters are close to $1.23 + \mathrm{i}1.11$ fm, corresponding to the η-nucleon scattering length of $0.50 + \mathrm{i}0.33$ fm, which is obtained in the three-body Faddeev calculations [35].

5. Conclusions

The total and differential cross-sections have been measured for the $\gamma d \to \pi^0 \eta d$ reaction at $E_\gamma < 1.15$ GeV. The total cross-section $\sigma(E_\gamma)$ is well-reproduced by the existing theoretical calculations with ηd final-state interaction (FSI). The differential cross-sections $d\sigma/dM_{\eta d}$ and $d\sigma/dM_{\pi d}$ are decomposed to $\gamma d \to \mathcal{R}_{\pi\pi d} \to \pi^0 \mathcal{R}_{\eta d}/\eta \mathcal{R}_{\pi d} \to \pi^0 \eta d$. A phenomenological analysis shows $a_{\eta d} = \pm(0.7^{+0.8}_{-0.6}) + \mathrm{i}(0.0^{+1.5}_{-0.0})$ fm, suggesting rather weak ηd attraction corresponding to ηN scattering length of $a_{\eta N} = 0.50 + \mathrm{i}0.33$ fm. No theoretical calculations reproduce rather flat angular distributions of deuteron emission. Sizable angular differential cross-sections are obtained at forward angles of deuteron emission not only for $\gamma d \to \pi^0 \eta d$, but also for $\gamma d \to \pi^0 d$ [39], $\gamma d \to \pi^0 \pi^0 d$ [40–42], and also $\gamma d \to \pi^0 \pi^0 \pi^0 d$ [43]. The details of the analysis and discussion can be found elsewhere [20, 21].

Acknowledgments

The authors express gratitude to the ELPH staff for assistance during the FOREST experiments. This work was supported in part by JSPS KAKENHI Grants Nos. 19002003, 24244022, 26400287, 19H01902, 19H05141, 19H05181, 21H00114, and 22H001240.

References

[1] C. DeTar, T. Kunihiro, *Phys. Rev. D* **39**, 2805 (1989).

[2] T. Hatsuda, M. Prakash, *Phys. Lett. B* **224**, 11 (1989).

[3] H. Nagahiro D. Jido, S. Hirenzaki, *Nucl. Phys. A* **761**, 92 (2005).

[4] D. Jido, E.E. Kolomeitsev, H. Nagahiro, S. Hirenzaki, *Nucl. Phys. A* **811**, 158 (2008).

[5] A. Khreptak, M. Skurzok, P. Moskal, *Front. Phys.* **11**, 1186457 (2023).

[6] M. Skurzok, P. Moskal, N.G. Kelkar, S. Hirenzaki, H. Nagahiro, N. Ikeno, *Phys. Lett. B* **782**, 6 (2018).

[7] S.D. Bass, P. Moskal, *Rev. Mod. Phys.* **91**, 015003 (2019).

[8] B. Mayer, A. Boudard, B. Fabbro, et al., *Phys. Rev. C* **53**, 2068 (1996).

[9] J. Smyrski, H.-H. Adam, A. Budzanowski et al., *Phys. Lett. B* **649**, 258 (2007).

[10] T. Mersmann, A. Khoukaz, M. Büscher et al., *Phys. Rev. Lett.* **98**, 242301 (2007).

[11] M. Pfeiffer, J. Ahrens, J.R.M. Annand et al., *Phys. Rev. Lett.* **92**, 252001 (2004).

[12] M. Pfeiffer, U. Thoma, H. van Pee et al., *Phys. Rev. Lett.* **94**, 049102 (2005).

[13] F. Pheron, J. Ahrens, J.R.M. Annand et al., *Phys. Lett. B* **709**, 21 (2012).

[14] B. Krusche, C. Wilkin, *Prog. Part. Nucl. Phys.* **80**, 43 (2014).

[15] Y. Maghrbi et al. (Crystal Ball at MAMI, TAPS, and A2 Collaborations), *Eur. Phys. J. A* **49**, 38 (2013).

[16] H. Calén, J. Dyring, K. Fransson et al., *Phys. Rev. Lett.* **79**, 2672 (1997).

[17] H. Calén, J. Dyring, K. Fransson et al., *Phys. Rev. Lett.* **80**, 2069 (1998).

[18] F. Hibou, C. Wilkin, A. Bergdolt et al., *Eur. Phys. J. A* **7**, 537 (2000).

[19] R. Bilger, W. Brodowski, H. Calén et al., *Phys. Rev. C* **69**, 014003 (2004).

[20] T. Ishikawa, H. Fujimura, H. Fukasawa et al., *Phys. Rev. C* **104**, L052201 (2021).

[21] T. Ishikawa, A. Fix, H. Fujimura et al., *Phys. Rev. C* **105**, 045201 (2022).

[22] T. Ishikawa, H. Fujimura, H. Fukasawa et al., *JPS Conf. Proc.* **10**, 031001 (2016).

[23] T. Ishikawa, H. Fujimura, R. Hashimoto et al., *Nucl. Instrum. Method A* **622**, 1 (2010).

[24] T. Ishikawa, H. Fujimura, H. Hamano et al., *Nucl. Instrum. Method A* **811**, 124 (2016).

[25] Y. Matsumura, T. Ishikawa, Y. Honda et al., *Nucl. Instrum. Method A* **902**, 103 (2018).

[26] Y. Obara, T. Ishikawa, H. Hama et al., *Nucl. Instrum. Method A* **922**, 108 (2019).

[27] H. Hama, *AAPPS Bull.* **30**, 41 (2020).

[28] Website of Research Center for Accelerator and Radioisotope Science.

[29] F. Hinode, H. Hama, M. Kawai et al., in: *Proc. of 21st IEEE Particle Accelerator Conf. (PAC)*, IEEE, Piscataway (NJ) 2005, p. 2458.

[30] T. Ishikawa, H. Fujimura, H. Fukasawa et al., *Nucl. Instrum. Method A* **832**, 108 (2016).

[31] S. Agostineli, J. Allison, K. Amako et al., *Nucl. Instrum. Method A* **506**, 250 (2003).

[32] J. Allison, K. Amako, J. Apostolakis et al., *IEEE Trans. Nucl. Sci.* **53**, 270 (2006).

[33] Geant4 website.

[34] A. Käser, J. Ahrens, J.R.M. Annand et al., *Phys. Lett. B* **748**, 244 (2015).

[35] M. Egorov, A. Fix, *Phys. Rev. C* **88**, 054611 (2013).

[36] M. Egorov, *Phys. Rev. C* **101**, 065205 (2020).

[37] A.J. Clara Figueiredo, T.C. Jude, S. Alef et al., arXiv:2405.09392, 2024.

[38] A. Martínez Torres, K.P. Khemchandani, E. Oset, *Phys. Rev. C* **107**, 025202 (2023).

[39] Y. Ilieva et al., (CLAS collaboration), *Eur. Phys. J. A* **43**, 261 (2010).

[40] T. Ishikawa, H. Fujimura, H. Fukasawa et al., *Phys. Lett. B* **772**, 398 (2017).

[41] T. Ishikawa, H. Fujimura, H. Fukasawa et al., *Phys. Lett. B* **789**, 413 (2019).

[42] T.C. Jude, S. Alef, R. Beck et al., *Phys. Lett. B* **832**, 137277 (2022).

[43] T. Ishikawa, talk at: *Exotic Multi-Quark States and Baryon Spectroscopy Workshop*, Rheinische Friedrich-Wilhelms-Universtät, Bonn 2024.